Shielded Transceiver RF Coil Array for Simultaneous PET-MRI

E. Solis[1,4], D. Tomasi[1], S. Junnarkar[3], D. Schlyer[1], P. Vaska[1], C. Woody[2], J-F. Pratte[3], P. O'Connor[3], and A. O. Rodriguez[4]
[1]*Medical Department,* [2]*Physics Department,* [3]*Instrumentation Division Brookhaven National Laboratory, Upton, NY, 11973, The USA.* [4]*Centro de Investigacion en Instrumentacion e Imagenologia Medica, Universidad Autonoma Metropolitana Iztapalapa, Mexico, DF 09340, Mexico**

Received on 17 April, 2008

The complementary information provided by combined MRI-PET modalities promises to facilitate metabolic investigations of complex physiological processes. We developed a radio frequency (RF) coil array that can operate in close proximity (2-mm radial distance) to a miniaturized PET camera insert for simultaneous PET-MRI of a rat brain at high magnetic fields (4 Tesla). All ferromagnetic components in the PET instrument were replaced with non-ferromagnetic components to minimize susceptibility artefacts in MRI, and optical fibres were used to connect the electronics of the PET camera to the acquisition system located outside the MRI scanner room. A passive electromagnetic shielding was developed to minimize the interference between the PET-electronics and MRI RF coil array. MR images of water phantoms and "ex-vivo" rat brains were collected in two different conditions: with and without PET acquisition. Similarly, PET data was acquired in two different conditions: with and without MRI pulses (RF and gradients). The MR images showed good uniform sensitivity profiles for all cases and 66% decrease in SNR for the shielded case. The PET and MRI datasets demonstrated that the electromagnetic shielding successfully minimizes the RF interference between the instruments, minimizing MRI artefacts and protecting the delicate components of the PET electronics from MRI RF pulses.

Keywords: MRI coil array; Hybrid system; PET/MRI

I. INTRODUCTION

The ability to combine magnetic resonance imaging (MRI) and positron emission tomography (PET) is essential to study brain metabolism with anatomical precision [1-4]. While PET can map brain function and metabolism with low spatial resolution (2-10mm) using radioactive tracers, MRI can provide high-resolution anatomical maps with low functional and metabolic specificity. Thus the simultaneous PET-MRI acquisition aims to overcome the limitations of each individual technique. However, a number of technical challenges have to be surmounted to successfully integrate PET and MRI because MRI is highly sensitive to magnetic field inhomogeneities resulting from magnetic/metallic components of the PET camera and electromagnetic waves produced by the PET electronics, and PET is sensitive to the MRI fields and RF pulses. Because photomultiplier tubes cannot operate in the vicinity of the high magnetic fields [5-7], previous attempts to integrate PET and MRI used non-magnetic scintillating PET detectors in the MRI scanner bore that were connected to external photomultiplier tubes through long optical fibres [8], which significantly reduce the efficiency for the detection of gamma rays [9]. Alternatively an MRI compatible PET insert could be based on a non-magnetic version of the miniaturized PET scanner for the conscious rat brain (RatCAP) [10-11]. Because the LSO scintillating crystals, silicon avalanche photodiodes (ADP), and the associated electronics performing front-end signal processing are highly integrated in this PET scanner (Fig. 1.b) can operate in high magnetic fields [12], photon carrying optical fibers connecting scintillating crystals and ADP-photodetectors are not needed. However, the close proximity (2cm) of the PET-electronics and the MRI RF coil leads to additional challenges because the digital signals in electronic modules of the RatCAP can introduce noise in MR images and the MRI RF pulses can affect the sensitive electronics of the RatCAP. Thus, the principal aim of this paper is to develop a mid-range saddle coil array (2-30 MHz-m) [13] for mouse imaging that allows to operate the RatCAP electronics and the MRI coil simultaneously with minimal interference at high magnetic fields (4 Tesla). Ex vivo and in vitro coil testing was performed with 4T whole-body MR imager. Phantom and rat's brain images were acquired to demonstrate its viability to generate high quality images with standard spin-echo sequences at high field MRI.

*Corresponding author: Alfredo O. Rodriguez, arog@xanum.uam.mx

II. METHODS

A. MRI compatible RatCAP

A complete description of the RatCAP can be found in [14-15]. Briefly, it consists of a 4 cm diameter ring containing 12 block detectors, each of which consists of a 4x8 array of 2.3x2.3x5mm^3 cerium-doped lutetium oxyorthosilicate (LSO) crystals with a matching array of ADP (Hamamatsu S8550). The APDs are read out with a custom-designed ASIC implemented in 0.18 mm CMOS technology for its small size, high level of integration and low power. The original version of the RatCAP was made up of both non-magnetic and magnetic components. The non-magnetic components were the LSO crystals, the aluminium housing, the kapton insulating sheet, and the silicon electronic components. Other parts contained magnetic materials and had to be specially made to allow their use in the MRI. These included the APDs which re-

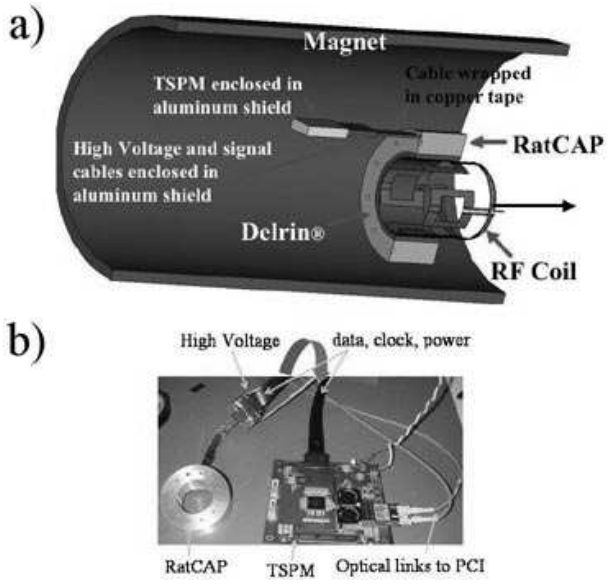

FIG. 1: a). Schematic showing the experimental setup for simultaneous PET and MR imaging showing the main components. The TSPM (Timestamp and Signal Processing Module) is the digital signal readout module. b). Photo of the electronics architecture of RatCaP showing parts.

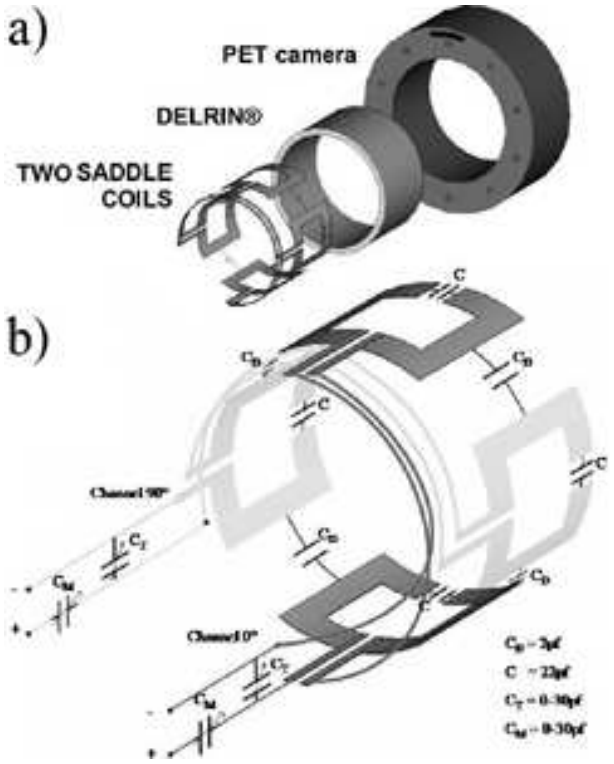

FIG. 2: Schematic diagram of transceiver coil array showing components and dimensions.

quired special non-magnetic pins, the APD sockets which had to be made without the steel pin sockets, a non-magnetic flex circuit board and non magnetic electronic components (e.g. solder leads). These components were shielded from the RF field by using a cylindrical aluminium housing surrounding the RatCAP. The Kapton cable carrying signals was shielded using copper tape. The entire data acquisition chain was then enclosed in an aluminium shield and set in the MR imager as shown in Fig. 2a) and 1a), respectively.

B. Electromagnetic modelling

The strong RF pulses used in MRI might interfere with the analog or digital signals (100 MHz clock) in the RatCAP and the RatCAP electronics can introduce RF noise in MRI. To avoid the interference between PET and MRI we used an electromagnetic shielding encasing the RatCAP (Fig. 2.a). To estimate the effect of the shielding in MRI we calculated the RF magnetic field, B1, produced by the coil array using a finite element method (FEM). Bi- and three-dimensional FEM models were used, to simulate the magnetic field for the unshielded and shielded conditions. All numerical computations of the electromagnetic field produced by coil configurations were carried out with the commercial software tool FEMLAB (COMSOL, Burlington, MA, USA). The following dimensions were used: saddle coil parameters: inner diameter of the of 2.35 cm, length of 2.3 cm and thickness of 0.65 cm, Delrin parameters: inner diameter of the of 3.3 cm, length of 2.3 cm and thickness of 0.3 cm, Shield parameters: inner diameter of the of 3.7 cm, length of 2.3 cm and thickness of 0.3 cm. The values of the specific conductivity and relative permittivity used for this calculation were those provided in the FEMLAB software: a) Saddle coils (copper): 5.998 107 S/m and 1 $Q^2/(Nm^2)$, b) Electrical insulation (Delrin(): 0 S/m and 2.9 $Q^2/(Nm^2)$, c) Shielding (aluminium): 3.774 107 S/m and 1 $Q^2/(Nm^2)$, and d) the sample: 0.5 S/m and 80 $Q^2/(Nm^2)$. Simulation parameters at 170MHz for a) saddle coil array, Delrin and no shielding: initialized mesh consists of 22759 elements, number of degrees of freedom: 34393, and solution time: 177.937 s. b) saddle coil array, Delrin and shielding: initialized mesh consists of 22053 elements, number of degrees of freedom solved for: 34740, and solution time: 30.719 s.

C. Transceiver array coil

A kapton printed circuit board (PCB) was used to build the transceiver RF coil array that simultaneously fit a rat head and the RatCAP scanner as shown in Fig. 6. The coil is based on two saddle coils [16] (inner diameter of 3.0 cm and length of 2.15 mm) working in quadrature configuration and mounted on a Delrin support. The coil array was operated in the transceiver mode. Each coil in the PCB was made of copper traces and four distributed capacitors of equal capacitance (2pF) to tune the coil and minimize electric field loss. Fig. 2.b) shows layout and electronic components. Two 50-Ω coaxial cables were attached to each RF channel. Variable capacitors (0-30pF; Voltronics, Denville, NJ) were used for tuning to 170.29 MHz (resonant frequency of the hydrogen) and 50-Ω matching. The coil was loaded with a cylindrical phantom (inner di-

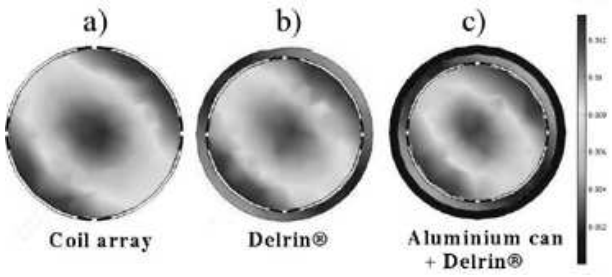

FIG. 3: Bi-dimensional maps of the magnetic field (B1) simulated with the FEM approach: a) the coil array, b) coil array and the Delrin ring, and c) the coil array, Delrin and the aluminium can.

ameter 2.5-cm, length 4-cm) filled with a 100-mM NaCl water solution, and the resonant frequencies were measured as the reflection coefficients (S11) by using a network analyzer and S-parameter test set (Model 4396A, Hewlett Packard, Palo Alto, CA, The USA), and quarter-wavelength coaxial cables. The resonant frequency, f, and its 3dB-bandwidth, Δf, were measured and the quality factor Q of the coil array was determined as $Q = \frac{f}{\Delta f}$. The rough estimate of the images SNR was computed by taking a ROI within the images and outside the images, and diving the mean of each ROI. This is a very crude way to measure the signal-to-noise ratio (SNR).

D. MRI acquisition

All experiments were carried out on a 4 Tesla Varian/Siemens MRI system equipped with a self-shielded whole-body SONATA gradient set. T1- and T2-weighted axial images of a cylindrical water phantom (2.5-cm inner diameter; 4 cm length; 1mM $CuSO_4$) and an "ex-vivo" rat head were acquired without the RatCAP scanner to evaluate image quality and SNR in the standard operation mode (without RatCAP). The experiments were repeated with the coil array inside the RatCAP in "ON" acquisition mode using a standard spin echo pulse sequence; in this mode the electronics of the RatCAP is operationally driven by a 100-MHz digital clock [14]. A complementary image was collected with the RatCAP "OFF" acquisition mode to evaluate the interference of the digital signals of the PET electronics on MRI.

III. RESULTS

The magnetic field of the coil array was simulated for three conditions: a) coil array, b) coil array surrounded by a Delrin ring, and c) coil array covered with the Delrin(ring and an aluminium can. Fig. 3 shows bi-dimensional images of the simulations performed at 170 MHz for the cases mentioned above. Resulting simulations show a great agreement with those numerical simulations reported in the literature [17-18].The aluminium can acts as a shielding to protect the PET electronics from the field produced by the coil array. The aluminium shielding affects drastically the coil array performance and

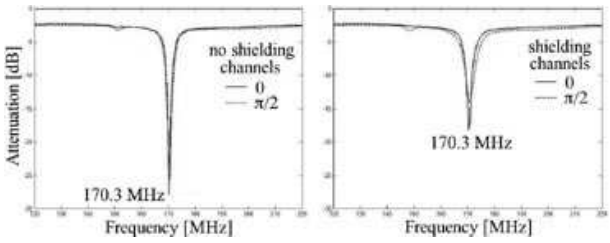

FIG. 4: Plots of loss return-vs-frequency for the coil for both channels (0^0 and 90^0) under the unshielded conditions (a), and inside the aluminium can (b).

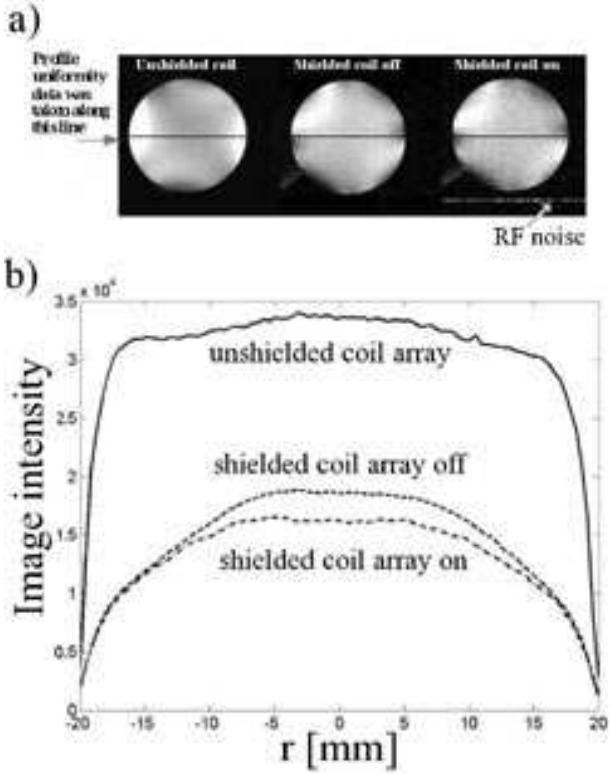

FIG. 5: Phantom image comparison acquired with the MRI PET system including the shielding and the unshielded cases. a) Delrin and coil only, b) Delrin and coil inserted in the RatCap off-case, and c) Delrin and coil inserted in the RatCap on-case. Comparison of uniformity profiles of the coil array for the unshielded case and the shielded case and the RatCAP turned off.

this can be appreciated in the quality factor measures. The coil array performance (Q factor) was measured for the following cases: a) the Q factor for the coil array and Delrin no load was 44, and b) the coil array, Delrin® and RatCap was approximately 21. Fig. 4 shows the loss return-vs-frequency plots for both channels (0^0 and 90^0) under the loaded and loaded conditions considering the shielded and unshielded case. Phantom images with the coil array and the RatCap were acquired using a spin-echo sequence for various cases. Fig. 5.a) shows phantom images acquired with the experimental setup of Fig. 1.a) for the following condition: the coil was inserted in the Delrin (and the aluminium can as shown in Fig. 2.a) and images

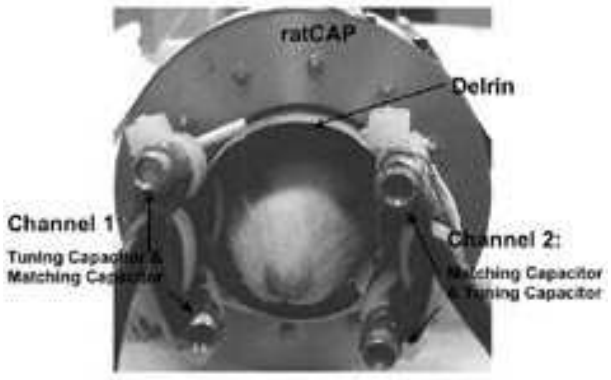

FIG. 6: Picture of experimental setup showing coil mounted inside the μPET and fitted on a rat head.

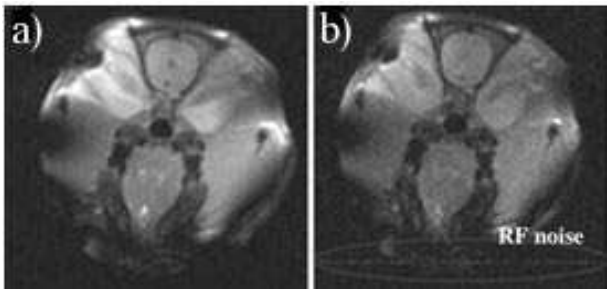

FIG. 7: Comparison of rat brain image: a) only coil array, and b) coil array inserted in the PET camera with PET data acquisition system running.

were acquired with the RatCap turned on and off. Uniformity profiles were also computed from phantom images for the shielded and unshielded case and shown in Fig. 5.b). The uniformity profiles in Fig. 5.b) demonstrate that the aluminum shielding reduced the SNR of the RF coil array by 66% for both RatCAP operating conditions (SNR ("Unshielded") = 61.7, SNR ("OFF") = 51.0, and SNR ("ON") = 24.0) of the RatCAP. These profiles show an important decrease in the SNR of the coil for the shielded case. However, the uniformity maintains a very similar pattern to the unshielded case. Simultaneous ex vivo image acquisition of rat brain were carried out with the RatCAP inserted into the bore of the BNL 4T human scanner as shown in Fig. 1a) with the experimental arrangement of Fig. 6. Images of Fig. 7 show that the aluminium can efficiently shield the RF signals (100 MHz clock) produced by the electronics modules in the miniaturized PET camera (mainly from the 100 MHz clock), which were only 2 cm distant from the MR image isocenter; the weak RF noise component resulting from the PET electronics did not compromise the quality of the MR images. However, the proximity (2mm) between the aluminium can and the RF coil array reduced the SNR three fold with respect to the unshielded case forcing to average a larger number of experiments for the required contrast to noise. The MR images showed minimum RF noise due the PET electronics despite the close proximity between the PET camera and the MRI RF coil. Similarly, the PET datasets demonstrated minimum propagation of RF-noise due to MRI RF pulses.

IV. DISCUSSION

The B1 field simulations showed that the magnetic field can be efficiently confined within the aluminium encasing and the Delrin(. These numerical results predict that the sensitive μPET camera electronics will no suffer any possible damage as a result of the magnetic fields generated by the RF pulses applied via the coil array. This is particularly important since the coil array was operated in the transceiver mode. This can be appreciated in both phantom and "ex vivo" images. According to Dotty [13] the saddle coil array presented in this paper can be considered a mid-range coil array since f (resonant frequency of protons) x d (coil array diameter) = 6.80 MHz-m, and this type of coils is relatively simple to develop. However, the coil array size imposed a great deal of effort to tune it properly to the correct resonant frequency. It is important to mention that 4 non-magnetic trimmers were necessary to add to the coil array (see Fig. 2b). This is a considerable source of noise if we consider that other 8 fixed-value capacitors were soldered too. Since the coil array was printed on a flexible board and then mounted on a plastic cylinder, construction imperfections did not greatly affect the image quality.The loss return plots (Fig. 4) showed an excellent agreement between the two channels (0^0 and 90^0) in terms of pattern and penetration for the unshielded case. This assures us that the same quality factor can be measured for both channels and that a pretty similar behaviour can be observed. This is particularly important for the quadrature drive to guarantee a good image quality. The coil array penetration suffers a 10 dB loss with the aluminium shielding that can be reflected in the image quality in the form of SNR loss. Mutual inductance effects can be appreciated in the form hypo-intensities near the perimeter of the phantom image. This is caused by the closed proximity of the coil elements. To attenuate this unwanted effects, capacitive coupling (C_D capacitors) was implemented between the coil elements as shown in Fig. 2.b). From the Fig. 5.a) phantom images can be observed that the capacitive coupling was able to attenuate this unwanted effect.Phantom T1-weighted images of Fig. 5a show a reasonably good image quality for all cases. The uniformity profile shows that a typical pattern with an acceptable uniformity. Uniformity results computed from phantom images showed that this coil designs is able to generate high quality phantom images with standard echo spin sequences. The shielding crucially affects the image SNR. This fact motivates the study of other materials to more efficiently shield the RF coil, which combined with other possible RF coils and coil arrays may attenuate the SNR loss in the image improving the quality of the study. Numerical simulations of the magnetic field can be of great assistance in this task.Finally, ex vivo mouse's brain images were also acquired (Fig. 7). Phantom images together with images of a mouse's brain proved the feasibility of the scaled version of a saddle coil array and, its compatibility with standard pulse sequences when used in a high field magnetic resonance imager.These

experimental results demonstrate that it is indeed possible to simultaneously acquire reasonable quality PET and MRI images employing the RatCAP and a shielded-saddle coil array. Neither the MRI nor the PET images displayed any artifacts attributable to the melding of the two imaging modalities. These results may pave the way for creation of more complex imagers that will permit continued study of this new area of multi-modality, complementary imaging.

Acknowledgement

S. S. is supported by a Ph D stipend from the National Council of Science and Technology of Mexico (CONACyT), and thanks Laboratory Directed Research and Development from U.S. Department of Energy (OBER). This work was supported by the U.S. Department of Energy (OBER) under Prime Contract No. DE-AC02-98CH10886. Support from Innovamedica is gratefully appreciated.

[1] H. Zaidi, Z. Med. Phys. **16**, 5 (2006).
[2] H. A. Wolbart, W. R. Hendee, Radiology. **238**, 16 (2006).
[3] S. R. Cherry, Annu. Rev. Biomed. Eng. **8**, 35 (2006).
[4] N. Volkow, B. Rosen, and L. Farde, Proc. Natl. Acad. Sci. USA. **94**, 2787 (1997).
[5] D. W. Townsend, S. R. Cherry, Eur. Radiol. **11**, 1968 (2001).
[6] P. K. Marsden, D. Strul, S. F. Keevil, S. C. Williams, and D. Cash, Br. J. Radiol. **75**, S53 (2002).
[7] Y. Shao, S. R. Cherry, K. Farahani, K. Meadors, S. Siegel, R. W. Silverman, and P. K. Marsden, Phys. Med. Biol. **42**, 1965 (1997).
[8] R. B. Slates, K. Farahani, Y. Shao, P. K. Marsden, J. Taylor, P. E. Summers, S. Williams, J. Beech, and S. R. Cherry, Phys. Med. Biol. **44**, 2015 (1999).
[9] Y. Shao, S. R. Cherry, K. Farahani, R. Slates, R. W. Silverman, K. Meadors, A. Bowery, S. Siegel, P. K. Marsden, and P. B. Garlick, IEEE Trans. Nucl. Med. **44**, 1167 (1997).
[10] P. Vaska, C. L. Woody, D. J. Schlyer, S. Shokouhi, S. P. Stoll, J. F. Pratte, P. O'Connor, S. S. Junnarkar, S. Rescia, B. Yu, M. Purschke, A. Kandasamay, A. Villanueva, A. Kriplani, V. Radeka, N. Volkow, R. Lecomte, and R. Fontaine, IEEE Trans. Nucl. Sci. **51**, 2718 (2004).
[11] S. Shokouhi, P. Vaska, D. J. Schlyer, S. P. Stoll, A. Villanueva, A. Kriplani, and C. L. Woody, IEEE Trans. Nucl. Sci. **52**, 1305 (2005).
[12] R. Slates, S. R. Cherry, A. Boutefnouchet, Y. Shao, M. Dahlbom, and K. Farahani, IEEE Trans. Nucl. Sci. **46**, 565 (1999).
[13] F. D. Doty, G. Entzminger, J. Kulkarni, K. Pamarthy, and J. P. Staab, NMR Biomed. **20**, 304 (2007).
[14] P. Vaska, C. L. Woody, D. J. Schlyer, S. Shokouhi, S. P. Stoll, J. F. Pratte, P. O'Connor, S. S. Junnarkar, S. Rescia, B. Yu, M. Purschke, A. Kandasamay, A. Villanueva, A. Kriplani, V. Radeka, N. Volkow, R. Lecomte, and R. Fontaine, IEEE Trans. Nucl. Sci. **51**, 2718 (2004).
[15] S. Shokouhi, P. Vaska, D. J. Schlyer, S. P. Stoll, and A. Villanueva, IEEE Trans. Nucl. Sci. **52**, 1305 (2005).
[16] D. I. Hoult, R. E. Richards, J. Magn. Reson. **24**, 71 (1976).
[17] W. T. Sobol, Rev. Magn. Reson. Med. **1**, 181 (1986).
[18] T. Claasen-Vujcic, H. M. Borsboom, H. J. G. Gaykema, and T. Mehlkopf, Magn. Reson. Med. **36**, 111 (1996).